

# 3D Printed Cubesat Propulsion Subsystem

A project present to  
The Faculty of the Department of Aerospace Engineering  
San Jose State University

in partial fulfillment of the requirements for the degree  
*Master of Science in Aerospace Engineering*

By

**Tyler Franklin**

May, 2018

approved by

Dr. P. Papadopoulos  
Faculty Advisor



To my parents, without them this would not be possible.

## ABSTRACT

### 3D PRINTED CUBESAT PROPULSION SUBSYSTEM

by Tyler Franklin

A 3D printable cold gas propulsion system for Cubesat attitude control has been designed. The system has four nozzles each capable of delivering 50 mN thrust at a theoretical vacuum specific impulse of  $60 \text{ s}^{-1}$  using DuPont 236fa refrigerant. The nozzles can be fired in any combination to initiate rotation around three different axes. The thruster can hold 117 g of propellant and depending on the chosen material has a dry mass of around 80g.

## Nomenclature

$P_1$	= The gas pressure in the source vessel at $t_1$
$P_2$	= The gas pressure in the source vessel at $t_2$
$t_1$	= Any time after flow starts
$t_2$	= Any time (later than $t_1$ ) after flow starts
$C$	= Coefficient of discharge
$A$	= Area of the source discharge
$V$	= Volume of the source vessel
$\gamma$	= $c_p / c_v$
$g$	= Gravitational acceleration
$R_s$	= Specific gas constant
$T_c$	= Chamber temperature
$P_c$	= Chamber pressure
$M$	= Mach number
$\rho$	= Density
$I_{sp}$	= Specific Impulse
$F_t$	= Thrust force
$A_e$	= Nozzle exit area
$A_t$	= Nozzle throat area
$V_e$	= Nozzle exit velocity
$V_{eq}$	= Nozzle equivalent velocity
$\dot{m}$	= Propellant mass flow rate

## TABLE OF CONTENTS

<b>1.0</b>	<b>INTRODUCTION &amp; MOTIVATION.....</b>	<b>11</b>
1.1	LITERATURE REVIEW .....	12
1.1.1	Additive Manufacturing .....	12
1.1.2	Stratasys uPrint SE Plus 3D Printer .....	13
1.1.3	Cold Gas Propulsion Systems .....	13
1.1.4	Warm Gas Propulsion Systems .....	18
1.1.5	Nozzle Flow Governing Equations .....	20
1.2	PROJECT PROPOSAL .....	21
1.3	METHODOLOGY .....	22
<b>2.0</b>	<b>PROPELLANT &amp; MATERIALS SELECTION .....</b>	<b>24</b>
2.1	Propellant Overview .....	24
2.2	Materials Overview .....	28
2.3	Selection .....	30
<b>3.0</b>	<b>DESIGN METHODOLOGY .....</b>	<b>30</b>
3.1	ISENTROPIC ANALYSIS .....	31

3.2	TRANSIENT PRESSURE DROP METHODOLOGY .....	32
3.3	STEADY STATE ANALYSIS .....	33
<b>4.0</b>	<b>DESIGN .....</b>	<b>34</b>
<b>5.0</b>	<b>NOZZLE ANALYSIS .....</b>	<b>40</b>
5.1	CFD Analysis .....	40
5.1.1	Fundamental Equations .....	40
5.1.2	Mesh .....	44
5.1.3	Model Setup .....	44
5.1.4	Results .....	44
5.2	Alternative Nozzle Arrangement .....	52
<b>6.0</b>	<b>CONCLUSION .....</b>	<b>53</b>
6.1	Future Work .....	54
<b>7.0</b>	<b>REFERENCES .....</b>	<b>55</b>

## TABLES

Table 1-1.	Bevo-2 Thruster Specifications [6] .....	16
Table 1-2.	Various Cold Gas Propellant Properties [7] .....	17
Table 2-1.	HFC 236fa Physical Properties [13] .....	25
Table 2-2.	R134a Physical Properties [15] .....	27
Table 3-1.	Steady State Inputs .....	34
Table 3-2.	Steady State Outputs .....	34

Table 4-1. Thruster Dry Mass.....	40
-----------------------------------	----

## TABLE OF FIGURES

Figure 1-1. Thruster Schematic [6] .....	15
Figure 1-2. RAMPART MEMS Resistojet Propulsion Schematic [10].....	19
Figure 1-3. 2D Nozzle Geometry .....	20
Figure 2-1. 236fa Plastic Compatibility .....	24
Figure 4-1. Thruster Side View .....	35
Figure 4-2. Thruster Isometric View .....	36
Figure 4-3. Transparent Side View .....	37
Figure 4-4. Transparent Isometric View .....	38
Figure 4-5. Transparent Side View with Plenum .....	38
Figure 4-6. Section View .....	39
Figure 5-1. Differential Element .....	41
Figure 5-2. Example Mesh .....	44
Figure 5-3. 45 Degree Single Nozzle Velocity Vector Field .....	45
Figure 5-4. 45 Degree Single Nozzle Pressure Distribution .....	45
Figure 5-5. 45 Degree Single Nozzle Upper Wall Pressure Distribution .....	46
Figure 5-6. 45 Degree Velocity Vector Field .....	47
Figure 5-7. 45 Degree Pressure Distribution .....	47
Figure 5-8. 45 Degree Nozzle Upper Wall Pressure Distribution .....	48

Figure 5-9. 30 Degree Single Nozzle Velocity Vector Field .....	48
Figure 5-10. 45 Degree Single Nozzle Upper Wall Pressure Distribution .....	49
Figure 5-11. 30 Degree Velocity Vector Field .....	49
Figure 5-12. 30 Degree Pressure Distribution .....	50
Figure 5-13. 30 Degree Nozzle Upper Wall Pressure Distribution .....	50
Figure 5-14. 30 Degree Extended Distance Velocity Vector Field .....	51
Figure 5-15. 30 Degree Extended Distance Pressure Distribution .....	51
Figure 5-16. 30 Degree Nozzle Extended Distance Upper Wall Pressure Distribution	52
Figure 5-17. Alternative Nozzle Arrangement .....	53

## 1.0 INTRODUCTION & MOTIVATION

The latest paradigm shift in satellite development has been towards tiny satellites known as Cubesats. A 1 unit Cubesat (1U) has dimensions 10 cm by 10 cm by 10 cm. Combining novel small electronic systems with such a small satellite platform has allowed for the development of experimental and commercial payloads at very low prices. Many institutions, such as high schools, universities, and “New Space” startups, have been easily able to develop Cubesats thanks to their low cost and ease of manufacture. Rapid technological development and commercialization in the field of additive manufacturing (3D printing) has the immense potential to further drive the simplicity and cost decrease of Cubesat system deployment. With the increase in Cubesat development comes the need for propulsion subsystem engineering. Propulsion capabilities are absolutely essential in increasing the mission proficiency of future Cubesats. Innovative and novel propulsion systems are needed to provide rotational/attitude control, orbit change, de-orbit, or provide delta-V, depending on the specific mission requirements. There are many different propulsion technologies currently in development for Cubesats. Cubesat propulsion can be divided into three major sections. Existing technologies such as butane systems, arc thrusters, and pulsed plasma thrusters. New thruster technologies under development such as monopropellant systems, green monopropellant systems, cold gas systems, and ion propulsion systems. The third area consists of emerging technologies that include electrospray and discharge propulsion [1]. This project seeks to explore a novel and innovative inquiry into additively manufactured propellant systems for the

purpose of attitude control of a Cubesat. Additive manufacturing would allow for ease of manufacture, lower cost, and a modular design that could be “plug-and-play”. Cold gas propulsion systems are a rapidly growing area of interest due to the fact that they are inert, non-toxic, cheap, simple, and reliable. Green monopropellant propulsion systems are also of interest due to their high thrust level and minimal complexity [2][3]. The literature survey in this report will analyze relevant research and technology pertaining to cold-gas and monopropellant propulsion systems. Section 1.1 contains the literature review. Section 1.2 describes the project objective, and section 1.3 describes the project methodology.

## **1.1 LITERATURE REVIEW**

### **1.1.1 Additive Manufacturing**

Additive manufacturing, or 3D printing, is a process in which a structure is constructed layer by layer. Parts and assemblies are able to be constructed with greater precision and complexity that would be much more difficult and costly to develop with traditional machining processes. One example is seen in Figure 1-1 which has volumes enclosed in a solid chunk of plastic. This sort of structure would be near impossible to create without a 3D printer. Additive manufacturing technology allows for easier manufacturing of cold gas thruster systems. Cold gas systems of the past require valves, piping volume, tank volume, and assembly access areas. Furthermore, each of these interfaces increases the chance of propellant leakage. 3D printing can solve this problem by printing the volumes and interfaces in a solid piece of material, therefore reducing leak chance.

A flight ready 3D printed thruster system can be produced for under \$1000 (cold

gas) and manufactured in less than a week [3]. 3D printers are able to print at resolutions on the order of hundredths of a millimeter, and allow for easy reconfiguration of a thruster module to be adapted to a specific host spacecraft platform [3].

#### 1.1.2 Stratasys uPrint SE Plus 3D Printer

The San Jose State University Aerospace Engineering department has a Stratasys uPrint SE Plus 3D printer. The uPrint SE Plus can provide a total build size of 8 x 8 x 6 inches, and has two layer thickness modes of .254 mm or .330 mm. It uses ABSplus (acrylonitrile butadiene styrene) thermoplastic as a material, and uses fused deposition modeling as its printing technique [4]. ABS is a plastic used to make Lego bricks, protective headgear, automotive components, and many other consumer goods. ABSplus is an enhanced version of ABS.

#### 1.1.3 Cold Gas Propulsion Systems

A microelectromechanical system (MEMS) picosatellite on STS-116 used a five thruster cold gas propulsion system [5]. The picosatellite measured 4 x 4 x 5 inches with a mass of 1.4 kg. The Aerospace Corporation used a method of manufacturing that was low cost, tightly integrated and leak proof. The manufacturing method used employed an additive manufacturing method known as stereolithography (SLA). A SLA printer was used to manufacture the propulsion system manifold which houses the propellant tank, plumbing, valves, and the converging diverging nozzle. The resin material chosen for the thruster structure was Somos 11120 resin. The entire thruster unit mass was 188 grams. The propellant used was DuPont SUVA HFC-236fa refrigerant and had the capability to deliver 20 m/s of delta-V to the 1.4 kg picosatellite.

A novel cold gas propulsion system for small satellites has been developed at University of Texas Austin's Satellite Design Lab [6], which was built upon the design concepts in [5]. The propulsion system is additively manufactured, allowing complex and intricate features. The system is operated by releasing saturated liquid propellant serially through three valves and a converging-diverging nozzle. Testing resulted in a system that provide a specific impulse range from 65 seconds at 24 Celsius to over 80 seconds at 85 Celsius. The measured thrust force range was measured from 110 mN to 150 mN, respectively. Without propellant, the system mass is 310 grams. The propellant used is DuPont 236-fa. 10 m/s of delta-v capability is expected to be provided by the system. Due to the fact that the entire thruster, main tank, secondary tank, internal piping, and converging-diverging nozzle are all encased in one block of plastic the time it takes to manufacture the system is very short and inexpensive compared to traditional counterparts. Furthermore, the design is modular. The nozzle can be placed anywhere on the satellite as needed. Many different propellants can be used without design change, including green propellants. The development of the system outlined in [6] is designed to be flown on a 3U Cubesat. The entire thruster system occupies a total volume of less than one half of a 1U Cubesat. Due to increased fidelity with 3D printing, it is easier to have fewer locations in the system with a possibility of leakage. The design has no waste volume for tooling to bend pipes or tighten nuts. The thruster can be printed, filled with propellant, sealed, and installed into the satellite system. Figure 1-1 shows the thruster schematic.

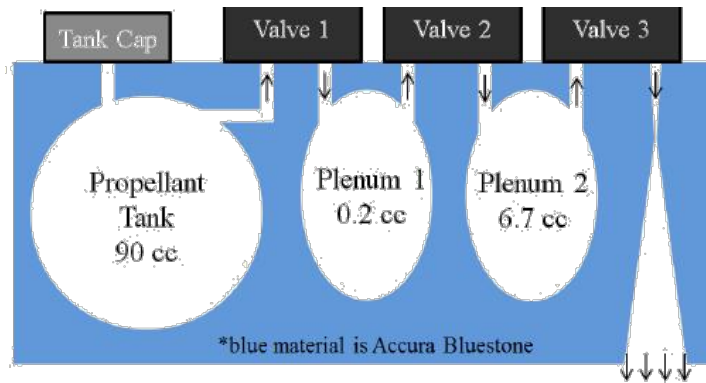


Figure 1-1. Thruster Schematic [6]

The system is entirely pressure driven, with the propellant stored as saturated liquid in the main tank. In the first plenum the propellant is two-phase liquid gas, and the second plenum is sized in a way that ensures the propellant resides in vapor form. This design has no active sensor measuring devices and is operated passively with two inputs. These inputs are the desired change in velocity and the ambient temperature. The thruster can function with the operating pressure of the chosen propellant. However, although higher vapor pressures result in higher performance, a stronger thruster material may be required. Lee Co valves were chosen because of their low power draw. The entire “Bevo-2” system can be manufactured for a cost of less than \$1000. Table 1-1 describes the Bevo-2 final system specifications.

Table 1-1. Bevo-2 Thruster Specifications [6]

Thruster System Characteristic	Value
Total dry mass	290 grams
Propellant mass	90 grams
Total thruster system mass	380 grams
Minimum power	0 W
Maximum power	1.5 W
Maximum valve operation pressure	800 psig
Valve actuation rate	500 Hz
Dimensions	10 x 9 x 4.4 cm

An AIAA paper from Uppsala University in Sweden examined the merits of cold gas micro propulsion systems [7]. The researchers found that cold gas is an excellent choice for missions that require extreme stabilization, pointing precision, or contamination free operation. Cold gas systems are simple in design, clean, safe, robust, and can operate on low power. Table 1-2 shows the properties of possible cold gas propellants.

Table 1-2. Various Cold Gas Propellant Properties [7]

$M_r$  = Molecular weight.  $t_m$  = Melting temperature.  $t_b$  = Boiling temperature.  $\rho$  = Density (241 bar, 0°C).  $I_{sp,t}$  = Theoretical specific impulse.  $I_{sp,m}$  = Measured specific impulse

Cold gas	$M_r$ kg/kmol	$t_m$ (1 bar) °C	$t_b$ (1 bar) °C	$\rho$ (241 bar) g/cm <sup>3</sup>	$I_{sp,t}$ <sup>a)</sup> s	$I_{sp,m}$ <sup>b)</sup> s
H <sub>2</sub>	2.0	-259	-253	0.02	296	272
He	4.0	-272	-269	0.04	179	165
Ne	20.4	-249	-246	0.19	82	75
N <sub>2</sub>	28	-210	-196	0.28	80	73
Ar	39.9	-189	-186	0.44	57	52
Kr	83.8	-157	-152	1.08	39	37
Xe	131.3	-112	-108	2.74 <sup>b)</sup>	31	28
CCl <sub>2</sub> F <sub>2</sub>	121	-158	-29.8	---	46 <sup>c)</sup>	37
CF <sub>4</sub>	88	-184	-128	0.96	55	45
CH <sub>4</sub>	16	-182.5	-161.5	0.19	114	105
NH <sub>3</sub>	17	-78	-33	Liquid	105	96
N <sub>2</sub> O	44	-91	-88	---	67 <sup>c)</sup>	61
C <sub>2</sub> H <sub>6</sub>	41.1	-187.7	-42.1	Liquid	---	---
C <sub>4</sub> H <sub>10</sub>	58.1	-138.3	-0.5	Liquid	---	---
CO <sub>2</sub>	44	---	-78 (S)	Liquid	67	61
SF <sub>6</sub>	146.1	---	-64(S)	---	---	---

<sup>a)</sup> At 25°C. Assume expansion to zero pressure in the case of the theoretical value.

<sup>b)</sup> Likely stored at lower pressure value (138 bar) to maximize propellant-to-tank weight ratio.

<sup>c)</sup> At 38°C (560R) and area ratio of 100.

(S) Sublimation

Xenon is an interesting propellant choice because it is heavy and inert, however due to its viscosity as a function of temperature relationship, xenon specific impulse can be inefficient as temperature increases beyond a certain range. Helium and nitrogen are lighter than xenon and provide higher specific impulse, but to be stored in liquid form cryogenics must be employed and this is more demanding. Propane and butane have been used in the past on microsattellites. However these are hazardous compounds. Carbon dioxide sublimates at -78 Celsius at 1 bar, and has a high specific impulse. Sulfur hexafluoride has a heavy molecular weight, and sublimates at -64 Celsius at 1 bar. It is non-toxic and non-flammable. Sulfur hexafluoride is a strong candidate for current propulsion systems under development [7].

In his Master's thesis at UT Austin, Travis Imken designed a 3D printed cold gas propulsion system for NASA JPL's INSPIRE project [9]. Imken's design was built upon the design in [3]. Imken took his design capabilities beyond the Bevo-2, which was just a passive thruster system. He designed a feedback control system and integrated electronics into the propulsion system. The same propellant was used as in [3], which was R236A, as well as the same 3D printed material, Accura Bluestone.

#### 1.1.4 Warm Gas Propulsion Systems

Warm gas propulsion systems are almost identical to cold gas, with the exception that the gas is run through some sort of heating element such as a resistance heater before entering the converging-diverging nozzle portion of the thruster. Heating the gas takes more electrical power, but increases the specific impulse of the propellant. Warm gas systems are often called "resistojet" propulsion.

A large consortium of individuals from various industrial companies and academic institutions developed the 2U RAMPART Cubesat. The purpose of the RAMPART is to certify warm gas propulsion subsystems, rapid prototyping, and magnetic stabilization for Cubesat orbital altitude adjustment [1010]. The propulsion system is designed to raise the spacecraft to an apogee of 1200 km from a circular orbit of 450 km. The system utilizes microelectromechanical systems (MEMS) technologies. The entire propulsion system is 1U and attaches to a 1U Cubesat bus to form the overall 2U RAMPART platform.

The RAMPART propulsion system was developed by Dr. Adam Huang and his graduate students at University of Arkansas. The resistojet configuration operates by

raising the propellants baseline specific impulse from 67s to 90s by adding heat energy prior to the propellant entering the nozzle. The propellant chosen was DuPont R-134a which is inert and non-toxic. Furthermore, R-134a is a compressed fluid and has a high boiling point of 247 K. The propellant is self-pressurizing at the design RAMPART operational temperature range, eliminating the need for pumps as temperature is all that is required to control pressure. Figure 1-2 displays the propulsion system schematic.

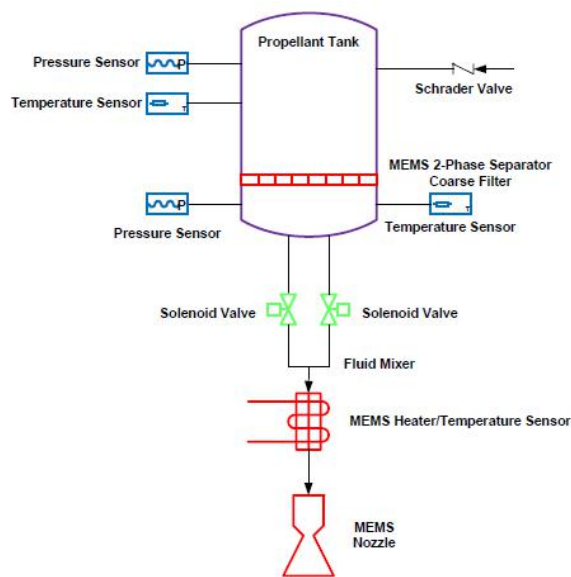


Figure 1-2. RAMPART MEMS Resistojet Propulsion Schematic [10]

The propellant tank is separated from downstream components by a MEMS membrane of porous channels that are 50 – 100  $\mu\text{m}$  diameter, etched by Deep Reactive Ion Etching (DRIE). This membrane prevents liquid phase fluid from being injected into the thruster. Gas phase propellant is controlled by a 2-way solenoid valve. The heater and nozzle assembly is composed of bonded silicon that is micro fabricated using MEMS technology. The nozzle has an expansion ratio of 50:1. Nozzle walls are designed as

adiabatic surfaces to minimize heat loss, which is typical in resistojets [7][8].

### 1.1.5 Nozzle Flow Governing Equations

The 2D geometry of a cold gas microthruster nozzle is shown in Figure 1-3 [11]. As subsonic gas enters the converging section its velocity increases, while in the divergent portion the supersonic gas increases in velocity. Therefore if the gas is sonic at the throat, it will continue to increase its velocity beyond the throat to supersonic values during nozzle expansion.

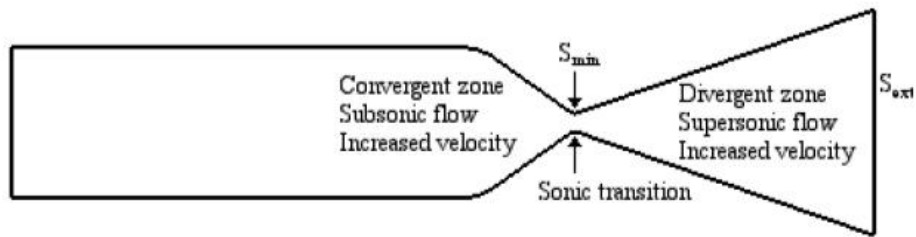


Figure 1-3. 2D Nozzle Geometry

To develop flow properties across the nozzle, 1D isentropic flow theory can be used. Beginning with the Euler equation (1), it is assumed the flow is only in the axial direction [8].

$$\rho \frac{dv}{dt} + (\rho v) \nabla = -\nabla p \quad (1)$$

Using conservation of mass with constant density, velocity, and cross sectional surface area, the continuity equation is shown in (2).

$$\frac{d\rho}{dt} + \rho \nabla v + \rho v \nabla = 0 \quad (2)$$

From (1) (2) and the speed of sound equation as a function of specific heat ratio, temperature, and molar mass, the rate of change of velocity with respect to area can be derived (3).

$$\frac{dv}{v} = -\frac{1}{2} \left( \frac{\gamma - 1}{\gamma + 1} \right) \frac{dA}{A} \quad (3)$$

C is speed of sound and M is the Mach number. From (3) it is seen that M is supersonic for dv/dA greater than zero. Velocity slows down for a convergent section where dA is less than zero and increases for the divergent portion with dA greater than zero. At the throat where dv/dA is zero, the flow is choked and the Mach number is one. Inserting the equation for adiabatic gas flow and the ideal gas equation into (1) gives the relation between Mach number and temperature (4).

$$\frac{T}{T_0} = 1 + \frac{\gamma - 1}{2} M^2 \quad (4)$$

Gamma is the specific heat ratio and T<sub>0</sub> is the reference temperature when flow velocity is zero. From (4) the adiabatic isentropic equations can be derived (5) (6).

$$\frac{\rho}{\rho_0} = \left( 1 + \frac{\gamma - 1}{2} M^2 \right)^{-\frac{1}{\gamma - 1}} \quad (5)$$

$$\frac{p}{p_0} = \left( 1 + \frac{\gamma - 1}{2} M^2 \right)^{-\frac{\gamma}{\gamma - 1}} \quad (6)$$

## 1.2 PROJECT PROPOSAL

The objective of this project is to design a cold gas propulsion system for an ambiguous Cubesat platform. The thruster will have a thrust of 50 mN per nozzle. The

propulsion system should be able to be printed with the Aerospace Engineering department uPrint SE Plus 3D printer. However, the printed prototype will not be for testing or flight purposes, as the uPrint SE Plus material ABSplus is not adequate for such applications. Regardless, the thruster will be designed to be printed and used with an appropriate material for flight operation should there be a desire to pursue future work. The printed prototype will be for “show and tell” purposes as a demonstrator of structure, modularity, scale, and form. The propulsion system will be designed and scaled for attitude control purposes, although the design and verification of a complete attitude control system is outside the scope of this project.

### **1.3 METHODOLOGY**

The first step in the propulsion system design methodology will be propellant down selection. A series of propellants will be examined based upon thermodynamic properties, safety, and efficiency. Both industrial refrigerants (such as DuPont) and elemental gases will be investigated. After propellant selection, design will commence on the thruster structure. A computer aided design tool such as SolidWorks will be utilized to draft the thruster. Although the thruster will not be printed for flight testing as described in section 1.2, it will be designed to be printed by an appropriate 3D printed material that could be used for testing and flight purposes, such as Accura Bluestone. In this way, should one want to pursue future work, the design could simply be sent to the appropriate additive manufacture and an experimental test model could be printed. A propellant pressure will be chosen based on propellant data and trade studies, and tanks will be sized using (6).

$$= \frac{\quad}{2} \tag{6}$$

Experimentally validating and testing the propulsion system is outside the scope of this project and therefore ANSYS Fluent will be used to validate the thruster properties and propellant flow. A control volume will be created around the converging-diverging nozzle portion of the thruster. Inlet nozzle pressure will be known, and ambient pressure will also be known. Fluent can numerically solve the Navier-Stokes equations in 2D and approximate a flow field. The software can integrate the dynamic pressure at the nozzle to get the axial force of the flow. This axial force is the thrust force delivered by the propulsion system onto the Cubesat. Mass flow rate at the nozzle exit will also be calculated by Fluent and specific impulse can be calculated from (7) [12].

$$= \frac{F}{m \cdot g_0} \quad (7)$$

Total system delta-v can be calculated using (8).

$$\Delta v = \sum \left( \frac{F}{m} \right) \cdot t \quad (8)$$

Due to the fact that a cold gas thruster does not require any additional power, the only power required will be to actuate valves. Appropriate benchmarks such as those in section 1.1 will be examined to help select appropriate valves to minimize power requirements. If adequate time is available, a warm gas thruster system will be investigated as a modification of the cold gas system. The methodology for warm gas thruster design will be very similar, with the bulk of the work being in regard to the resistor design or sourcing.

## 2.0 PROPELLANT & MATERIALS SELECTION

### 2.1 Propellant Overview

DuPont hydrofluorocarbon (HFC) 236fa is used as a cold gas propellant in both [5] and [6]. HFC 236fa was developed as an alternative to chlorofluorocarbon based fire suppression agents and refrigeration agents. The chemical formula is  $\text{CF}_3\text{CH}_2\text{CF}_3$  and it has a molecular weight of 152.04 g/mol. It is used by the U.S. Navy for refrigeration applications, and in various fire retardation equipment. Due to its low toxicity and thermodynamic properties, it is being used and investigated for cold gas propulsion systems. 236fa has been tested on certain plastics. These plastics were sprayed with 236fa and then their weight gain and surface alterations were examined. Results of the plastic compatibility testing is shown in Figure 2-1. The plastic that the SJSU uPrint uses, ABS, passed the test.

Plastic	Weight Gain (percent)	Surface Condition
High-density polyethylene (HDPE)	<1	No Change
Polystyrene (PS)	<1	No Change
Polypropylene (PP)	<1	No Change
Acrylonitrile-butadiene-styrene (ABS)	<1	No Change
Polycarbonate (PC)	<1	No Change
Polymethyl methacrylate (PMMA)	<1	No Change

Figure 2-1. 236fa Plastic Compatibility

Furthermore, R236fa was sealed in a 3D printed SLA propellant tank for 9 months for Bevo-2 thruster testing. The plastic showed no signs of deformation [9]. Table 2-1 shows the physical properties of 236fa. 236fa has a boiling point of 29.4°F, and is stored and transported as a liquefied compressed gas. A liquefied gas is defined as gas which

in packaging under the charged pressure is partially liquid at 20°C. Although 236fa is quite heavy when compared to elemental gases such as nitrogen and helium, it has favorable vapor pressure properties such that certification as a pressure vessel under NASA guidelines can be avoided. NASA regulations dictate that any sealed container greater than 100 psi is a pressure vessel, and a waiver must be obtained to launch as a secondary payload with NASA [14]. The vapor pressure of 236fa is 100 psi at 56°C, therefore a system utilizing 236fa and wishing to launch with NASA must maintain a temperature below 56°C to avoid such certification procedures.

Table 2-1. HFC 236fa Physical Properties [13]

Property	Value
Molecular Weight	152.04
Boiling Point (1 atm), °C (°F)	-1.4 (29.4)
Freezing Point, °C (°F)	-103 (-153)
Critical Temperature, °C (°F)	124.9 (256.9)
Critical Pressure, kPa (psia)	3200 (464)
Critical Density, kg/m <sup>3</sup> (lb/ft <sup>3</sup> )	555.3 (35.29)
Liquid Density @ 25°C (77°F), kg/m <sup>3</sup> (lb/ft <sup>3</sup> )	1360 (84.89)
Vapor Density @ 25°C (77°F) and 1 atm, kg/m <sup>3</sup> (lb/ft <sup>3</sup> )	6.430 (0.4014)
Specific Heat, Liquid @ 25°C (77°F), kJ/kg °C (Btu/lb °F)	1.1085 (0.3022)
Specific Heat, Vapor @ 25°C (77°F) and 1 atm, kJ/kg °C (Btu/lb °F)	0.8444 (0.2007)
Vapor Pressure, Saturated @ 25°C (77°F), kPa (psia)	272.4 (39.5)
Heat of Vaporization @ Boiling Point, kJ/kg (Btu/lb)	160.4 (68.97)
Thermal Conductivity, Liquid @ 25°C (77°F), W/m°C (Btu/hr-ft°F)	0.0745 (0.1289)
Thermal Conductivity, Vapor @ 25°C (77°F), W/m°C (Btu/hr-ft°F)	0.0042 (0.0073)
Viscosity, Liquid @ 25°C (77°F), Pa·s (lb-hr/ft <sup>2</sup> )	3.060E-04 (1.775E-09)
Relative dielectric strength @1 atm @760 mmHg, 25°C (N <sub>2</sub> =1)	1.0166
Solubility of Water in HFC-236fa @ 20°C (68°F), ppm	740
Solubility of HFC-236fa in Water @ 20°C (68°F), ppm	2,100
Ozone-Depletion Potential (CFC-11 = 1)	0.0
Halocarbon Global Warming Potential (CFC-11 = 1)	4.2
Global Warming Potential (GWP) (100 yr ITH. for CO <sub>2</sub> , GWP = 1)	6,300
TSCA Inventory Status	Reported, Included
SNAP Status	Listed
Inhalation Exposure Limit	AEL=1000 ppm (v/v) (8- and 12-hr TWA)

Another cold gas propellant of interest is also produced by DuPont, R134a (tetrafluoroethane). Much like 236fa, it was developed as an alternative to

chlorofluorocarbon based refrigerants. It has molecular formula  $\text{CH}_2\text{FCF}_3$  and a molecular weight of 102 g/mol [15]. It is nontoxic and inert and has been used in at least one small satellite propellant application, the RAMPART propulsion system [10]. Although the RAMPART system is a warm gas propulsion system, R134a could still be considered for a cold gas system. The RAMPART team chose R134a because it is FDA approved regarding inertness and toxicity. It has zero potential of flammability and does not leave residual contaminants that would affect other systems in the event of a burst or leak. One key parameter of R134a is that it is a compressed fluid. This is different from a cryogenic fluid in that its relatively high molecular weight results in a high boiling point of 247 K. That is to say for systems with high operating temperatures R134a could be self-pressurizing. Table 2-2 displays the physical properties of R134a. At 100 psi, the saturated temperature of R134a is around 37°C. The room temperature pressure of R134a is 85.9 psia.

Table 2-2. R134a Physical Properties [15]

Physical Property	Unit	Freon™ 134a
Chemical Name	—	Ethane, 1,1,1,2-Tetrafluoro
Chemical Formula	—	CH <sub>2</sub> FCF <sub>3</sub>
Molecular Weight	g/mol	102.03
Boiling Point at 1 atm (101.3 kPa or 1.013 bar)	°C °F	-26.1 -14.9
Freezing Point	°C °F	-103.3 213.9
Critical Temperature	°C °F	101.1 213.9
Critical Pressure	kPa psia	4060 588.9
Critical Volume	m <sup>3</sup> /kg ft <sup>3</sup> /lb	1.94 x 10 <sup>-3</sup> 0.031
Critical Density	kg/m <sup>3</sup> lb/ft <sup>3</sup>	515.3 32.17
Density (Liquid) at 25 °C (77 °F)	kg/m <sup>3</sup> lb/ft <sup>3</sup>	1,206 75.28
Density (Saturated Vapor) at Boiling Point	kg/m <sup>3</sup> lb/ft <sup>3</sup>	5.25 0.328
Heat Capacity (Liquid) at 25 °C (77 °F)	kJ/kg-K Btu/lb-(°F)	1.44 0.339
Heat Capacity (Vapor at Constant Pressure) at 25 °C (77 °F) (1 atm) (101.3 kPa or 1.013 bar)	kJ/kg-K Btu/lb-(°F)	0.852 0.204
Vapor Pressure at 25 °C (77 °F)	kPa bar psia	666.1 6.661 96.61
Heat of Vaporization at Normal Boiling Point	kJ/kg Btu/lb	217.2 93.4
Thermal Conductivity at 25 °C (77 °F) Liquid	W/m-K Btu/hr-ft-(°F)	0.0824 0.0478
Vapor at 1 atm (101.3 kPa or 1.013 bar)	W/m-K Btu/hr-ft-(°F)	0.0145 0.00836
Viscosity at 25 °C (77 °F) Liquid	MPa-S (cP)	0.202
Vapor at 1 atm (101.3 kPa or 1.013 bar)	MPa-S (cP)	0.012

Plastic compatibility tests were also conducted with R134a. ABS plastic results are listed as “needing more testing” for a conclusion. Reference [10] does not state which 3D printer or 3D printing material the RAMPART thruster was designed to use, nor has RAMPART ever flown. Therefore the compatibility of R134a with 3D printed plastics can only be surmised.

DuPont R123 has also been considered in cold gas propellant applications [9]. It has molecular formula CF<sub>3</sub>CHCl<sub>3</sub> and a molecular weight of 152.93 g/mol. It is relatively

nontoxic and inert like the other DuPont refrigerants. It has a room temperature pressure of 11.4 psia [16], and is easier to handle at room temperature because the saturation pressure is below atmospheric pressure, therefore it could be kept as a liquid during loading. However, the reduced pressure of R123 compared to the other DuPont refrigerants means that it will deliver less thrust at a given temperature. In regards to plastic material compatibility testing, ABS plastic is dissolved when submitted to liquid R123 at high temperatures.

The final DuPont refrigerant of interest is R124. It has a molecular weight of 136.48, and is inert and nontoxic. It has a room temperature pressure of 49 psia [17]. It is incompatible with ABS plastic.

## **2.2 Materials Overview**

The SJSU aerospace department 3D printer uses ABSplus plastic as its FDM filament. Although it is stated in section 1.3 that the objective of this project is not to print a final testable product, but instead to investigate the overall design of the propulsion system, due diligence should still be employed to investigate the compatibility of ABSplus plastic with the system requirements and the compatibility of the possible propellants listed in section 2.1. ABSplus is an amorphous plastic with a density of  $1.04 \text{ g/cm}^3$  with a printing accuracy of .01 inches. It has a tensile strength of 33 MPa, a modulus of elasticity of 2200 MPa, and 6% elongation at break [18]. Due to its amorphous nature, it does not have a specific melting point. Furthermore, the gaseous permeability of the proposed propellants with ABSplus is unknown.

Previous 3D printed cold gas propulsion systems have utilized the Accura 28

Bluestone material [5] [9]. Bluestone is a SLA nanocomposite plastic with a printing accuracy of .004 inches. It has a density of  $1.78 \text{ g/cm}^3$  and a tensile strength of 66 MPa. Its modulus of elasticity is 7600 MPa and has around 2.4% elongation at break. Furthermore, it has been shown to possess compatibility with certain DuPont refrigerants and Xenon [19]. Bluestone is specifically manufactured by the company 3D Systems for their ProX 800 printer.

Another material of interest to aerospace applications is Accura Ceramax. It has a room temperature density of  $1.62 \text{ g/cm}^3$  and a tensile modulus of 9460 MPa. It has the highest stiffness of all the 3D Systems materials as well as excellent chemical and thermal resistance. Although Ceramax has a lower density than Bluestone, it is more expensive [20]. Somos Nanotool is also a material that could be considered for thruster system applications. It has similar properties of Ceramax and it can be printed at half the layer thickness of Bluestone.

There are many different 3D printed materials that could be investigated and analyzed, but the bottom line is that the material chosen won't affect the design all that much. Due to the fact that this is a cold gas system temperatures will not be that high and most plastics should be able to withstand any proposed temperature range. The greatest concerns with the material selection will be potential permeability of the propellant through the material structure itself and the printing accuracy capable with the material. Most mechanical stresses would be expected to be quite low for such a small simple thruster design and should be well within the tolerances of most materials. The greatest performance parameter the material selection will impact will be thrust-to-weight ratio of

the system.

### **2.3 Selection**

The primary propellant for this design will be the DuPont 236fa refrigerant. Its desirable thermodynamic properties along with inertness and nontoxicity make it an ideal propellant for a cold gas system. It has proven compatible with Bluestone, and could possibly also be compatible with other SLA materials. Preliminary tests also show it is nonreactive with ABS plastic. The material chosen for the reference design will be Accura Bluestone. It is the only proven material for DuPont 236fa as shown in previous studies and designs. However, it will be explored to keep dimensioning within tolerances of ABSplus plastic so that a demonstrator thruster can be adequately printed using the SJSU aerospace department 3D printer.

### **3.0 DESIGN METHODOLOGY**

Developing an analytical methodology to describe the physics of a cold gas propulsion system is a challenging process. It is actually more difficult than a typical bi-propellant combustion analysis due to the fact that the cold gas propulsion system is entirely pressure driven. The cold gas is stored in its propellant tank under pressure, and a valve system is used to release the propellant through the converging diverging nozzle. After each “venting”, the pressure in the propellant tank changes which also changes the mass flow rate on the next vent and ultimately the exit pressure and the thrust. Therefore the cold gas system is an unsteady flow system.

This chapter will describe the isentropic equations used to setup the initial system conditions and a methodology that attempts to describe the system pressure drop.

### 3.1 ISENTROPIC ANALYSIS

The process begins by prescribing six design inputs. They are the propellant tank pressure  $P_c$ , the propellant tank temperature  $T_c$ , the propellant specific impulse, the nozzle thrust force, the nozzle throat area  $A_t$ , and the nozzle expansion ratio  $\epsilon_e$ . The area ratio Mach number relation is described by (9). This equation is a quadratic that can be solved numerically for Mach number or Mach numbers can be simply looked up for a given area ratio in tables in any compressible flow textbook.  $A_t$  is nozzle throat area,  $M_e$  is Mach number at the exit, and  $\gamma$  is the ratio of specific heats.

$$\frac{A}{A_t} = \frac{1}{M} \left[ \frac{2 + (\gamma - 1)M^2}{\gamma + 1} \right]^{\frac{\gamma + 1}{2(\gamma - 1)}} \quad (9)$$

Once the exit Mach number is known, the exit pressure  $P_e$  can be calculated from (10). Next the exit velocity  $v_e$  can be found from (11).

$$\frac{P_e}{P_c} = \left[ \frac{1 + \frac{\gamma - 1}{2} M_e^2}{\gamma + 1} \right]^{-\frac{\gamma}{\gamma - 1}} \quad (10)$$

$$v_e = \sqrt{\frac{2\gamma}{\gamma - 1} \left[ \frac{P_c}{\rho_c} \right] \left[ 1 - \left( \frac{P_e}{P_c} \right)^{\frac{\gamma - 1}{\gamma}} \right]} \quad (11)$$

Using the prescribed specific impulse and thrust, equivalent velocity and mass flow rate can be found with (12) and (13)

$$v_e = \frac{I_{sp} g_0}{\gamma} \quad (12)$$

$$= \dot{\quad} \quad (13)$$

### 3.2 TRANSIENT PRESSURE DROP METHODOLOGY

It can be seen in section 3.1 that for a system in which the tank pressure is not kept constant, unsteady flow occurs. Changing tank pressure changes the nozzle exit pressure and therefore changes the mass flow rate and ultimately the thrust. One way to try and approximate a change in pressure over a specified time interval is by using the integral form of conservation of mass with the ideal gas equation. This reduces to (16), where  $P_0$  is some initial pressure,  $Q$  is the volumetric flow rate of the gas,  $t$  is time, and  $V$  is the tank volume. This equation assumes that mass flow rate between the two pressures is constant. However it is not. Therefore this equation can only be used for very small time steps or thrust intervals where the pressure change is small enough to assume no significant change in mass flow. Furthermore this equation neglects any heat loss.

$$= \frac{\quad}{\quad} \quad (14)$$

The Rasouli-Williams source model equation is shown in (17) [21]. This equation was derived for choked gas flows from a pressurized gas system. Major assumptions made in its derivation include isothermal flow and a neutrally buoyant gas.

$$\frac{P_2}{P_1} = \left( \frac{t_2 - t_1}{t_2} \right)^{\frac{2}{\gamma - 1}} \quad (15)$$

Where:

- $P_1$  = the gas pressure in the source vessel at  $t_1$
- $P_2$  = the gas pressure in the source vessel at  $t_2$
- $t_1$  = any time after flow starts
- = any time (later than  $t_1$ ) after flow starts

C = coefficient of discharge  
A = area of the source discharge  
V= volume of the source vessel  
 $\gamma = C_p / C_v$   
g= gravitational acceleration  
R<sub>s</sub>= specific gas constant  
T<sub>c</sub>= initial gas temperature in the source vessel  
P<sub>c</sub>= initial gas pressure in the source vessel

Equation (17) requires a pressure at some time t after the flow begins, the very quantity wished to be solved for. It is possible to use (16) with a very small time step to approximate this P<sub>1</sub>. Furthermore the coefficient of discharge is hard to estimate properly for this situation and therefore results from (17) will always have a large degree of approximation. The analytical tools available for hand calculation for such a system are simply inferior to anything able to be produced by a full fidelity Navier-Stokes solver such as ANSYS Fluent or similar.

There is one way to change the system design so that isentropic equations will hold for each “thruster pulse” and that is by using some sort of electro-thermal heater to maintain a constant pressure in the propellant tank. Section 3.3 shows example inputs and outputs using section 3.1 methodology for such a steady state system.

### **3.3 STEADY STATE ANALYSIS**

Table 3-1 shows example inputs for a cold gas thruster system that uses a heater to maintain a constant temperature and pressure in the propellant tank. These properties including the value of gamma are representative of a typical R236 system [22]. Feeding these inputs through the equations shown in section 3.1 yields the results described in Table 3-2.

Table 3-1. Steady State Inputs

Parameter	Value	Units
Tank Pressure	263400	Pa
Tank Temp	297	K
Gamma	1.06	N/A
Isp	60	1/s
Molecular Weight	152.04	g/mol
Thrust	50	mN
Throat Radius	.001	m
Area Ratio	50	N/A

Table 3-2. Steady State Outputs

Parameter	Value	Units
Ve	1859	m/s
Ve <sub>q</sub>	568	m/s
Exit Radius	.007	m
Mass Flow Rate	8.50E-5	kg/s
Exit Mach	3.62	N/A
Exit Pressure	81839	Pa

Any desired thrust level can be achieved by adjusting the nozzle area ratio for a given set of propellant conditions.

## 4.0 DESIGN

This section describes the overall thruster system design and component arrangement. The thruster has a length of 10 cm, a width of 7.9 cm, and a thickness of 2.5 cm. The computer-aided-design (CAD) software used to model the thruster system was Dassault Solidworks. Figure 4-1 shows the thruster side view. Figure 4-2 shows the isometric view of the thruster. There are four nozzles in total which have a nozzle half angle of 45 degrees and are angled at 45 degrees relative to the structure. Any of these nozzles can be used in combination with each other to create rotation around the x, y, or z

z axis. Two of these nozzles can be seen in the isometric view. All of the nozzles have a throat radius of 1 mm, an exit radius of 7 mm, and provide a thrust of 50 mN. The left face with the 10 openings seen in the isometric view are the openings for the various flow pathways. This is where the valves and the valve manifolds would be mounted. The valve chosen for this design is the Lee Company IEP series solenoid valve. It is designed for high pressure applications and was also the valve chosen for many of the designs described in section 1.1.3. It should be noted that no screw bores have been included in the model below, however room has been allocated in the design to accommodate them.

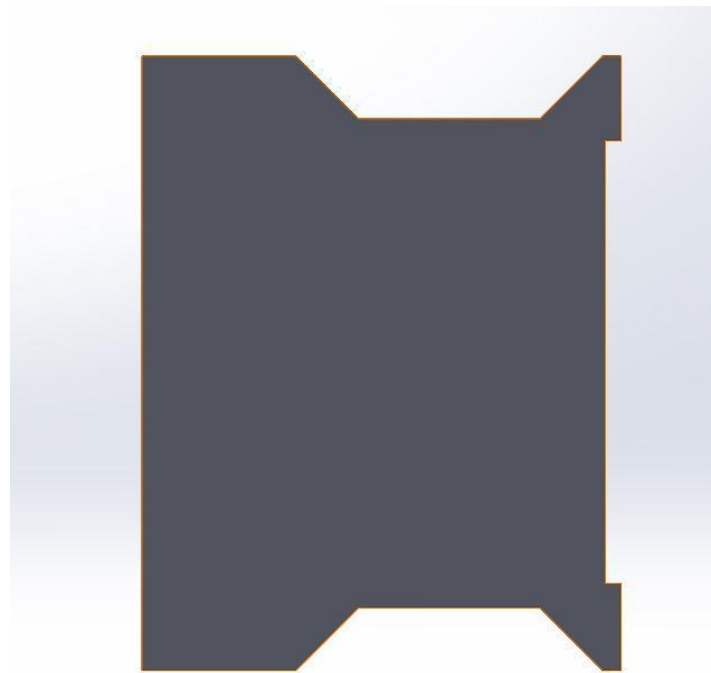


Figure 4-1. Thruster Side View

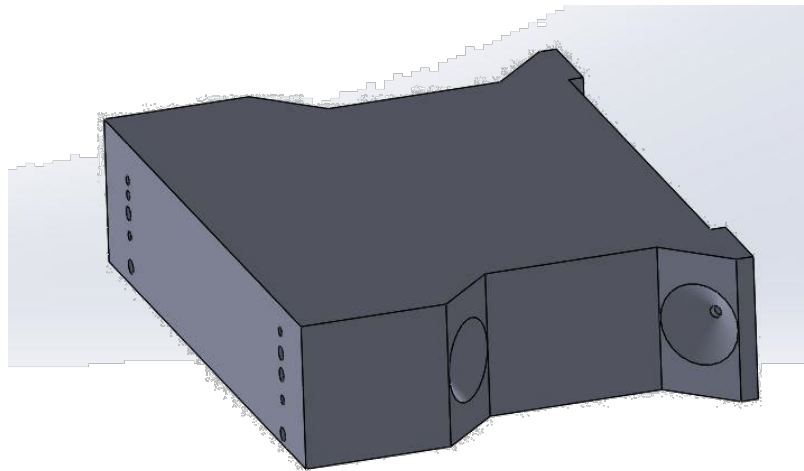


Figure 4-2. Thruster Isometric View

Figure 4-3 displays a side view of the thruster with the external face made transparent. The main propellant tank can be seen as well as the various pipes which connect the propellant plenum to the nozzles and the propellant tank. A transparent isometric view is pictured in Figure 4-4. This figure helps demonstrate how the internal tank attempts to use the maximum internal volume available. Figure 4-5 contains another side view with the external and propellant tank surfaces made transparent in order to view the spherical propellant plenum tank which sits inside the propellant tank. This plenum is sized in such a way to change the saturated liquid-gas mixture in the propellant tank into a gas before entering any of the four nozzles. The main propellant tank can store 117 grams of propellant. A section view of the thruster is shown in Figure 4-6 to demonstrate how the various components are hollowed out of the main thruster block. This is a unique feature of a 3D printed design which allows for ease of manufacture.

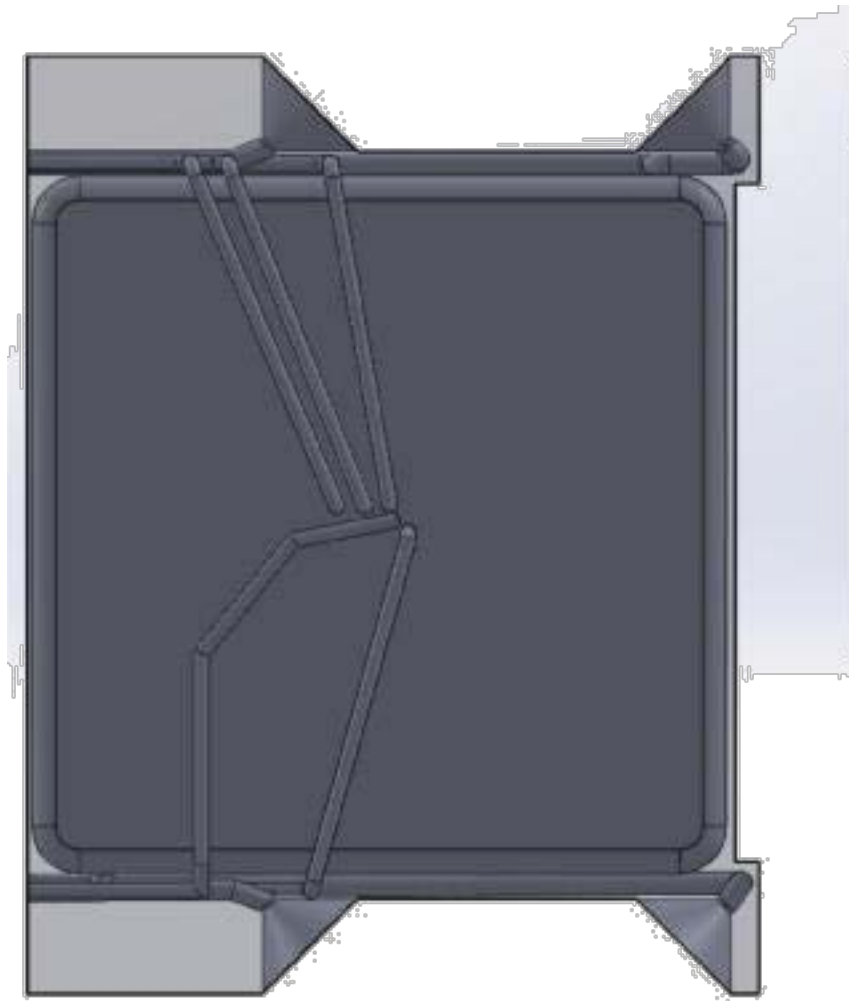


Figure 4-3. Transparent Side View

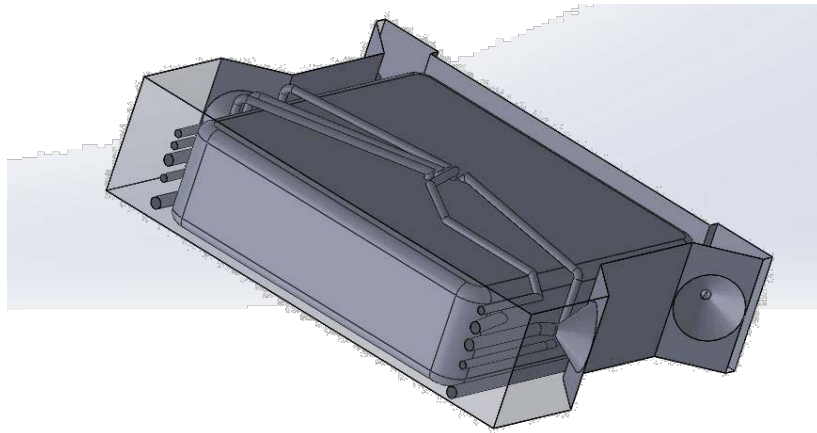


Figure 4-4. Transparent Isometric View

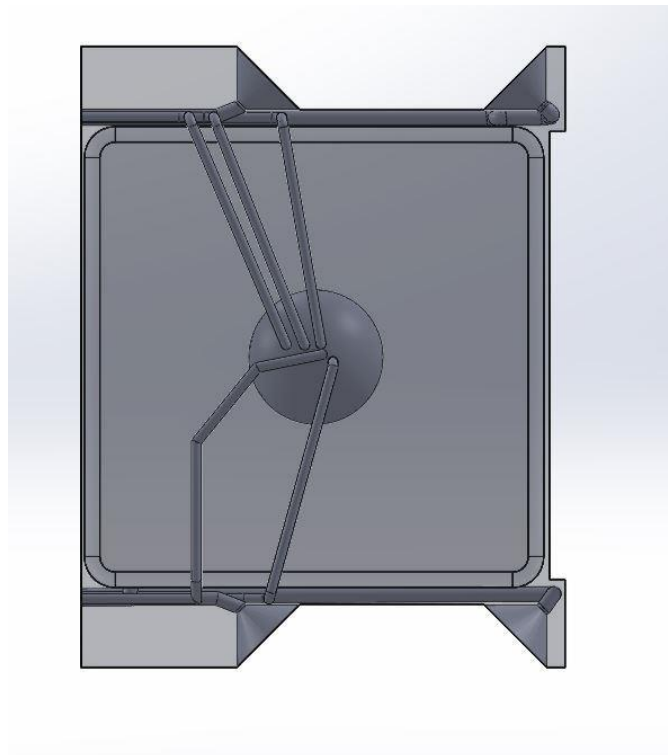


Figure 4-5. Transparent Side View with Plenum

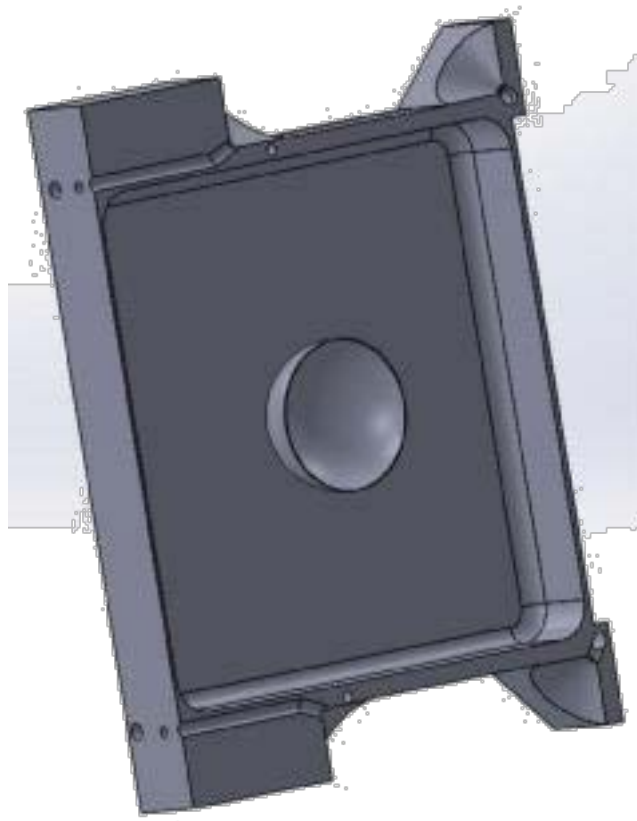


Figure 4-6. Section View

Table 4-1 shows the thruster dry mass for various printable materials. These materials and their properties are described in detail in section 2.2. The strongest and most expensive thruster would be one that uses Accura Ceramax. The lightest, cheapest, and weakest would be a design that uses ABSplus. A design that uses Accura Bluestone would be the safest choice as this material is proven to be compatible with the propellant as described in section 2. The overall small dry mass values for all materials can be attributed to the fact that the interior of thruster is mostly hollow due to the large propellant tank.

Table 4-1. Thruster Dry Mass

<b>Material</b>	<b>Dry Mass (g)</b>
ABSplus	51.34
Accura Bluestone	87.88
Accura Ceramax	79.98
Somos NanoTool	81.46

## **5.0 NOZZLE ANALYSIS**

Angled nozzles must be used to provide three degrees of freedom in a four nozzle design. The nozzles shown in section 4.0 are angled at 45 degrees. However, their arrangement could result in forces from the nozzle flow on the upper structural wall separating the two nozzles, as well as flow impingement of one nozzle on the other. Therefore computational fluid dynamic (CFD) analysis will be performed using the software ESI-Fastran.

### **5.1 CFD Analysis**

#### **5.1.1 Fundamental Equations**

ESI Fastran is a Navier-Stokes equation solver. The Navier-Stokes equations are the governing equations for fluid flow. The fundamental assumption in deriving the Navier-Stokes equations is that the fluid is made up of a continuous substance and is not discretized. The equations are derived from conservation of mass, conservation of momentum, and conservation of energy. The first step in the derivation is considering a differential element of fluid with a length  $dx$ , a height  $dy$ , and a depth  $dz$ . This is shown in Figure 5-1.

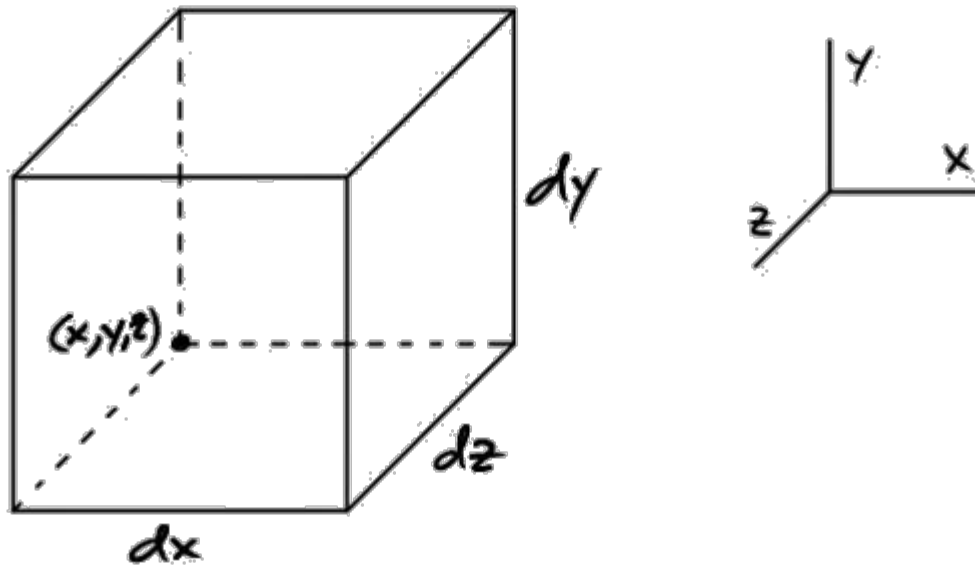


Figure 5-1. Differential Element

The first force we consider on the fluid element is the force of gravity. This is written as the mass of the fluid multiplied by the x component of gravity, which is equal to the density multiplied by the volume of the differential element of the fluid shown in (16).

$$= \tag{16}$$

Next we look at forces acting on the left and right side of our fluid element. There would be normal stresses acting on each face. One of these normal stresses is evaluated at a point  $x$ , while the other is evaluated at a point  $x+dx$ . This notation is shown in (17).

$$\sigma(x) \tag{17}$$

On the top and bottom faces there are shear stresses acting in opposite directions. The bottom shear stress is acting at some point  $y$  and the top shear stress is acting at some point  $y+dy$ . This notation is shown in (18).

$$\tau_{xy} - \tau_{yx} = \rho \frac{d}{dt} \left( \frac{1}{2} \rho \frac{d}{dt} \right) \quad (18)$$

Likewise there are shear stresses acting on the front and back faces of the cube in opposite directions (19).

$$\tau_{yz} - \tau_{zy} = \rho \frac{d}{dt} \left( \frac{1}{2} \rho \frac{d}{dt} \right) \quad (19)$$

Summing the forces in the x direction equal to the product of mass and acceleration on our differential fluid element yields (20), where mass is shown as the product of density and volume.

$$\tau_{xy} - \tau_{yx} + \tau_{yz} - \tau_{zy} + \tau_{zx} - \tau_{xz} = \rho \frac{d}{dt} \left( \frac{1}{2} \rho \frac{d}{dt} \right) \quad (20)$$

Dividing (20) by the volume of the element  $dx dy dz$  results in (21).

$$\frac{\tau_{xy} - \tau_{yx}}{dx dy dz} + \frac{\tau_{yz} - \tau_{zy}}{dx dy dz} + \frac{\tau_{zx} - \tau_{xz}}{dx dy dz} = \rho \frac{d}{dt} \left( \frac{1}{2} \rho \frac{d}{dt} \right) \quad (21)$$

Taking the limit of (21) with  $dx$ ,  $dy$ , and  $dz$  approaching 0 we get the differential form (22), with the acceleration component expanded into its local and convective components.

$$\frac{\partial \tau_{xy}}{\partial y} - \frac{\partial \tau_{yx}}{\partial x} + \frac{\partial \tau_{yz}}{\partial z} - \frac{\partial \tau_{zy}}{\partial y} + \frac{\partial \tau_{zx}}{\partial z} - \frac{\partial \tau_{xz}}{\partial x} = \rho \left( \frac{d}{dt} \frac{d}{dt} + \frac{d}{dt} \frac{d}{dt} + \frac{d}{dt} \frac{d}{dt} + \frac{d}{dt} \frac{d}{dt} \right) \quad (22)$$

Repeating this process for the other two directions results in (23) and (24). These three equations are the differential equations of motion for a fluid.

$$\frac{\partial \tau_{xy}}{\partial y} - \frac{\partial \tau_{yx}}{\partial x} + \frac{\partial \tau_{yz}}{\partial z} - \frac{\partial \tau_{zy}}{\partial y} + \frac{\partial \tau_{zx}}{\partial z} - \frac{\partial \tau_{xz}}{\partial x} = \rho \left( \frac{d}{dt} \frac{d}{dt} + \frac{d}{dt} \frac{d}{dt} + \frac{d}{dt} \frac{d}{dt} + \frac{d}{dt} \frac{d}{dt} \right) \quad (23)$$

$$+ \text{---} + \text{---} + \text{---} = ( \text{---} + \text{---} + \text{---} + \text{---} ) \quad (24)$$

To get from these equations to the Navier-Stokes equations we need a way to relate the normal and shear stresses to the viscosity of the fluid and the velocity profiles. This is done by using the constitutive equations for a Newtonian fluid shown in (25).

$$\begin{aligned} \sigma_{xx} &= -p + 2\mu \frac{\partial u}{\partial x} & \tau_{xy} &= \tau_{yx} = \mu \left( \frac{\partial u}{\partial y} + \frac{\partial v}{\partial x} \right) \\ \sigma_{yy} &= -p + 2\mu \frac{\partial v}{\partial y} & \tau_{yz} &= \tau_{zy} = \mu \left( \frac{\partial v}{\partial z} + \frac{\partial w}{\partial y} \right) \\ \sigma_{zz} &= -p + 2\mu \frac{\partial w}{\partial z} & \tau_{zx} &= \tau_{xz} = \mu \left( \frac{\partial w}{\partial x} + \frac{\partial u}{\partial z} \right) \end{aligned} \quad (25)$$

Substituting the relations from (25) into (22) (23) and (24) and differentiating will yield the Navier-Stokes equations (26).

$$\begin{aligned} \rho \left( \frac{\partial u}{\partial t} + u \frac{\partial u}{\partial x} + v \frac{\partial u}{\partial y} + w \frac{\partial u}{\partial z} \right) &= \rho g_x - \frac{\partial P}{\partial x} + \mu \left( \frac{\partial^2 u}{\partial x^2} + \frac{\partial^2 u}{\partial y^2} + \frac{\partial^2 u}{\partial z^2} \right) \\ \rho \left( \frac{\partial v}{\partial t} + u \frac{\partial v}{\partial x} + v \frac{\partial v}{\partial y} + w \frac{\partial v}{\partial z} \right) &= \rho g_y - \frac{\partial P}{\partial y} + \mu \left( \frac{\partial^2 v}{\partial x^2} + \frac{\partial^2 v}{\partial y^2} + \frac{\partial^2 v}{\partial z^2} \right) \\ \rho \left( \frac{\partial w}{\partial t} + u \frac{\partial w}{\partial x} + v \frac{\partial w}{\partial y} + w \frac{\partial w}{\partial z} \right) &= \rho g_z - \frac{\partial P}{\partial z} + \mu \left( \frac{\partial^2 w}{\partial x^2} + \frac{\partial^2 w}{\partial y^2} + \frac{\partial^2 w}{\partial z^2} \right) \end{aligned} \quad (26)$$

### 5.1.2 Mesh

A structured mesh was developed using ESI-Geom that has 1800 cells. Figure 5-2 displays an example mesh used. The flow analysis begins at the nozzle throat.

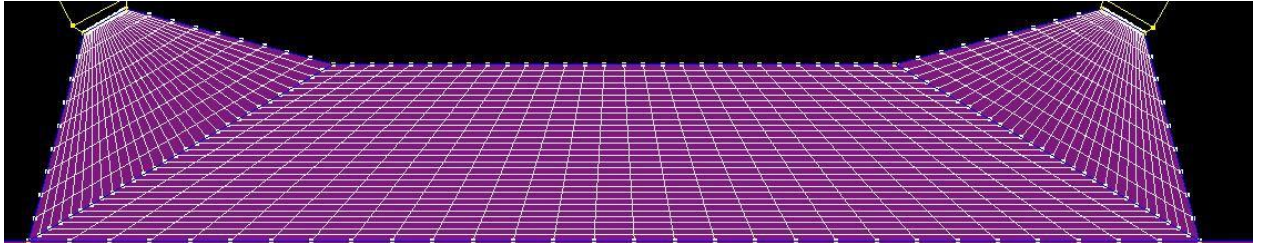


Figure 5-2. Example Mesh

### 5.1.3 Model Setup

All the volumes are initialized at vacuum pressure and 230 Kelvin to simulate vacuum conditions. The boundary conditions at the nozzle throat are simply calculated from the isentropic equations. They are set as inlet temperature and pressure conditions at 313 K and 172573 Pa. The far field is setup as a vacuum outlet. The simulation is run at steady state using a standard laminar flow solver for 3000 iterations until converged.

### 5.1.4 Results

Before the effects of both nozzles firing at once can be completely understood, a single nozzle firing must be analyzed. Figure 5-3 shows the velocity vector profile for a single 45 degree nozzle in operation. It can easily be seen that large amounts of the flow end up in the other nozzle as well as along the upper wall between the two nozzles.

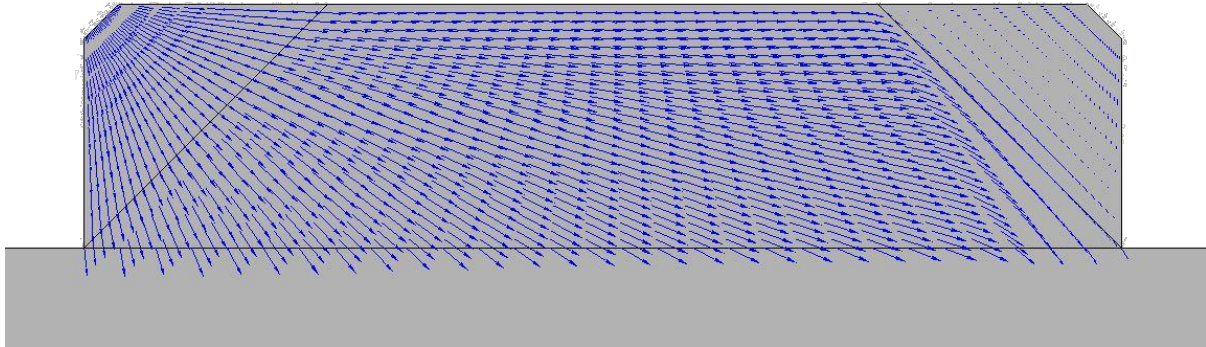


Figure 5-3. 45 Degree Single Nozzle Velocity Vector Field

The pressure distribution for single nozzle operation is seen in Figure 5-4. It shows large flow forces on the inactive nozzle. Figure 5-5 shows the pressure forces along the length of the upper wall between the two nozzles. The pressure is highest at the edge of the nozzle-wall interface on both sides. An optimized propulsion system should not have any flow pressure on its own structure.

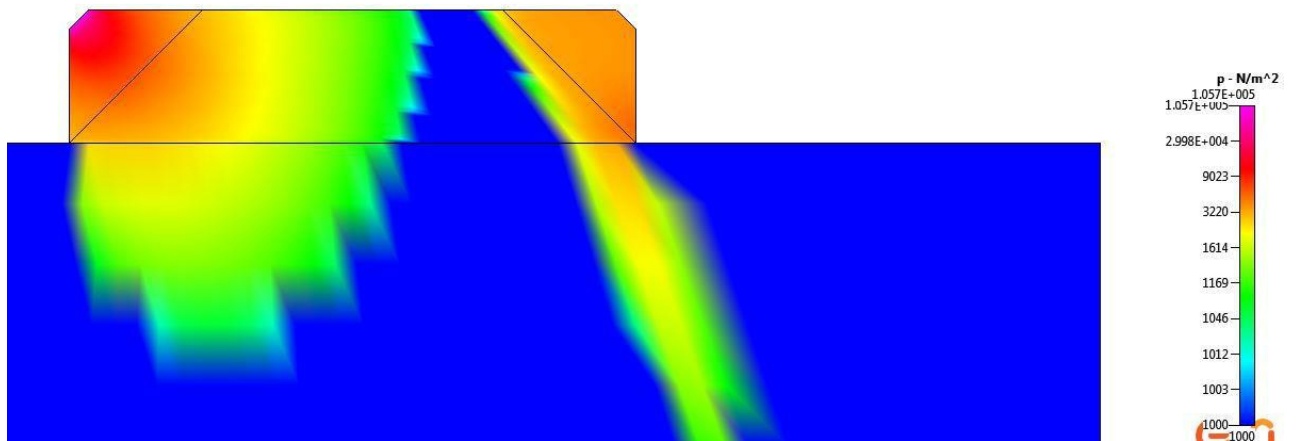


Figure 5-4. 45 Degree Single Nozzle Pressure Distribution

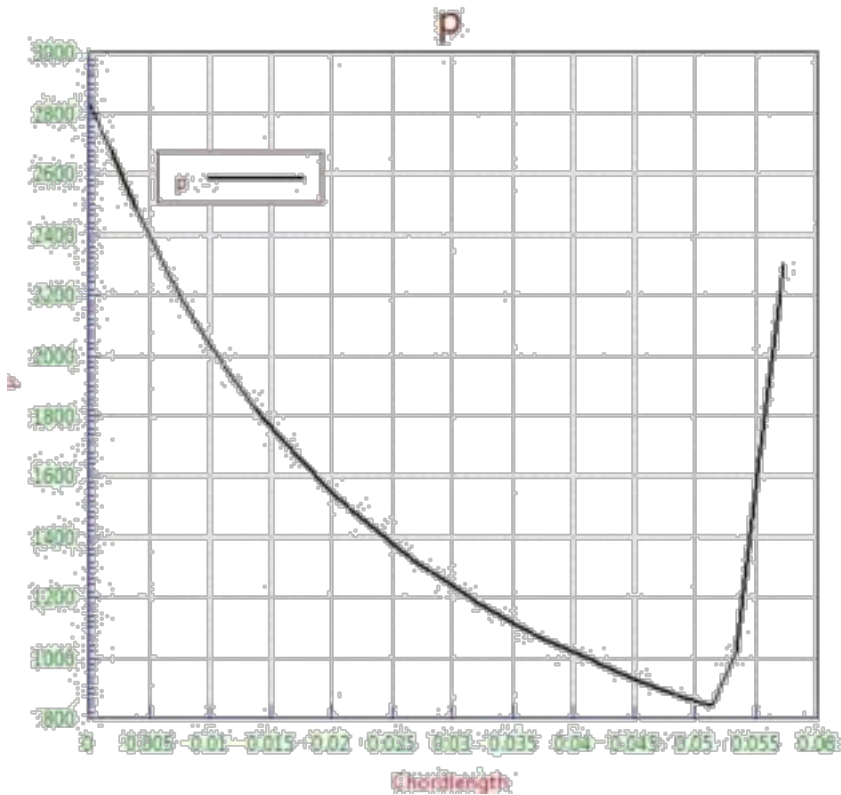


Figure 5-5. 45 Degree Single Nozzle Upper Wall Pressure Distribution

Figure 5-6 shows the velocity vector field for two 45 degree nozzles in operation. Flow interaction between the two nozzles is clearly seen in the middle of the image. Figure 5-7 shows the pressure distribution for the same case. The flow has very high pressure where the two flows interact and mix in the dark red upper center of the figure. These results show that this nozzle configuration is less than optimal when both nozzles fire at the same time.

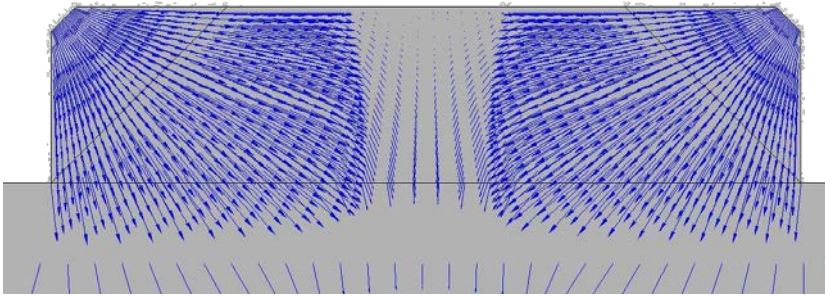


Figure 5-6. 45 Degree Velocity Vector Field

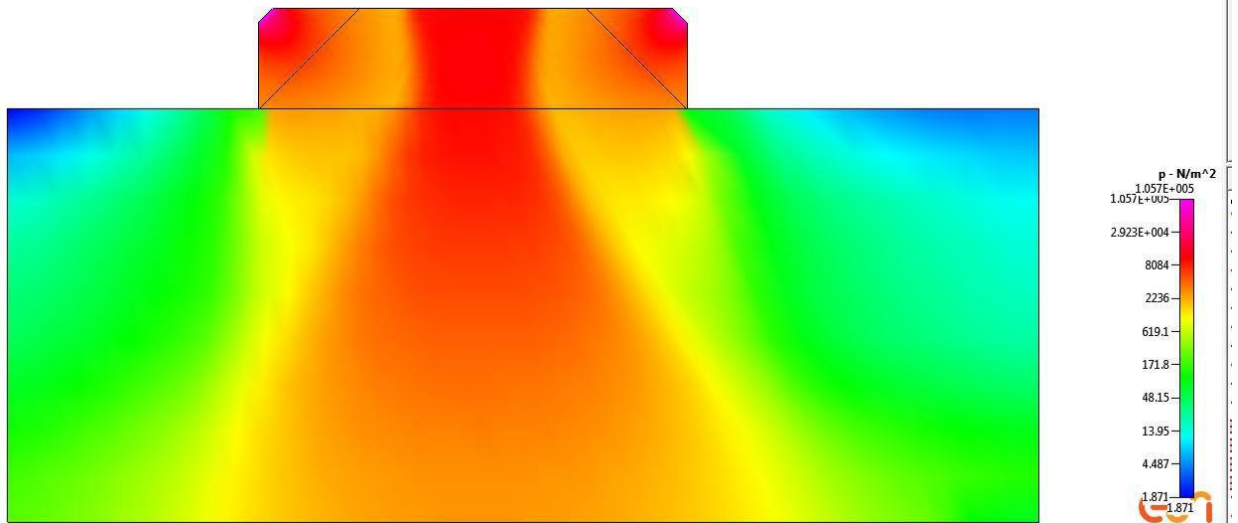


Figure 5-7. 45 Degree Pressure Distribution

The pressure distribution along the length of the upper wall between the two nozzles is displayed in Figure 5-8. The pressure peaks in the middle at around 10900 Pa.

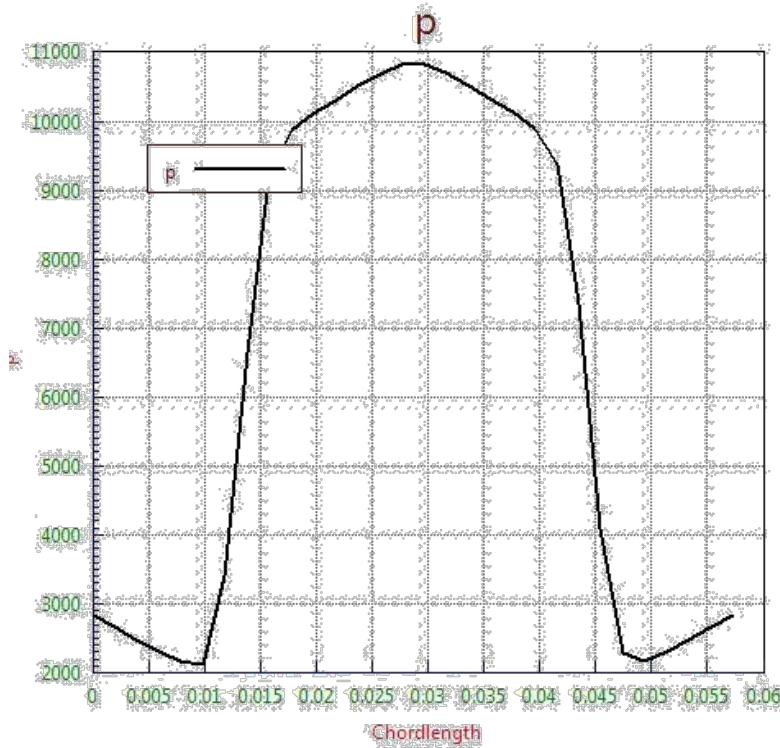


Figure 5-8. 45 Degree Nozzle Upper Wall Pressure Distribution

An alternative configuration with the nozzles angled at 30 degrees was simulated. The velocity vector field for a single 30 degree nozzle operation is shown in Figure 5-9. Much of the flow is directed into the thruster structure and the other nozzle.

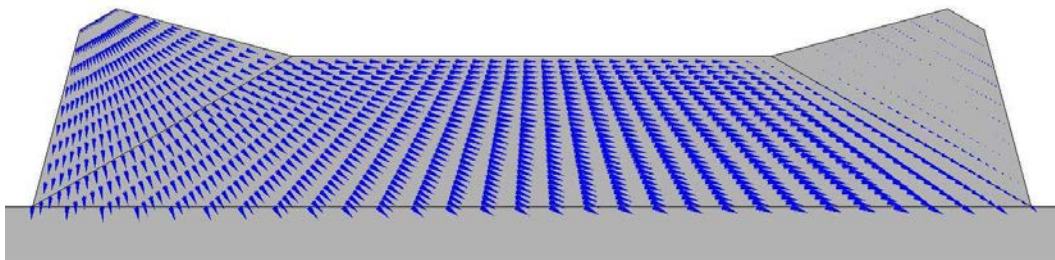


Figure 5-9. 30 Degree Single Nozzle Velocity Vector Field

The upper structure wall pressure distribution is displayed in Figure 5-10. The pressure peaks at the nozzle exit and decreases along the wall until it rises once the flow enters

the other nozzle.

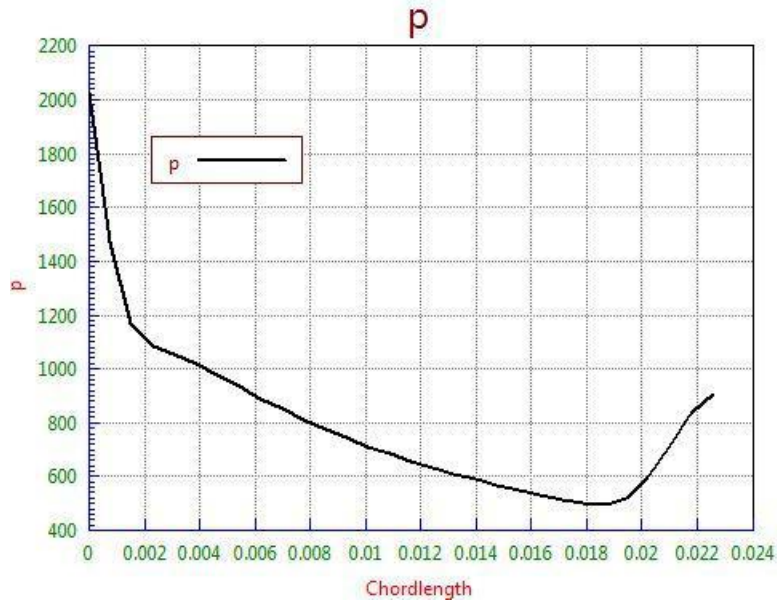


Figure 5-10. 45 Degree Single Nozzle Upper Wall Pressure Distribution

Figure 5-11 shows the velocity vector field for both 30 degree nozzles in operation. The flow can be seen interacting about half way between the two nozzles.

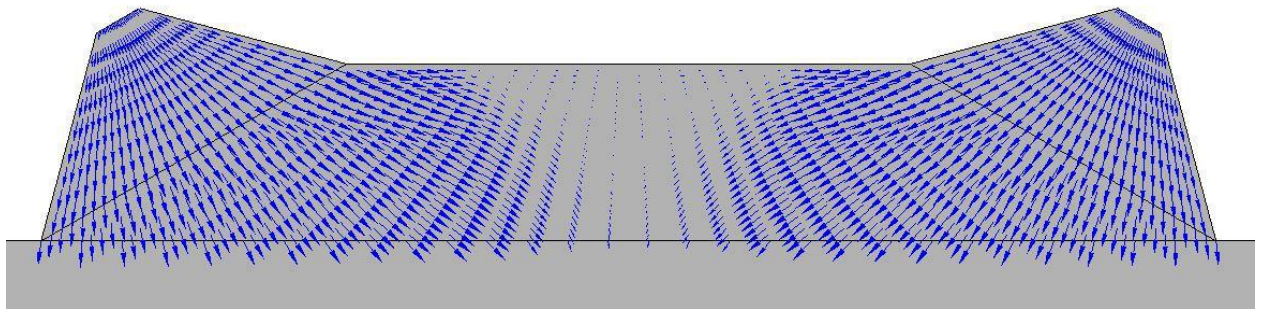


Figure 5-11. 30 Degree Velocity Vector Field

The pressure distribution for both 30 degree nozzles in operation is shown in Figure 5-12. Similarly to the 45 degree case, a region of high pressure due to nozzle flow

is seen in the upper middle along the structural wall.

Figure 5-13 shows the upper

wall pressure distribution. The same trend as the 45 degree case is observed with the pressure building to about half way between the two nozzles and peaking at 5700 Pa.

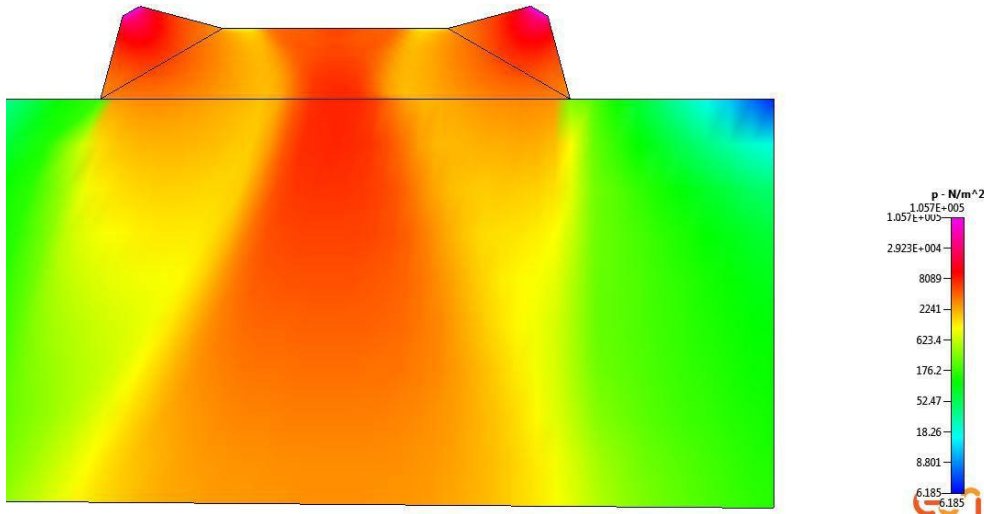


Figure 5-12. 30 Degree Pressure Distribution

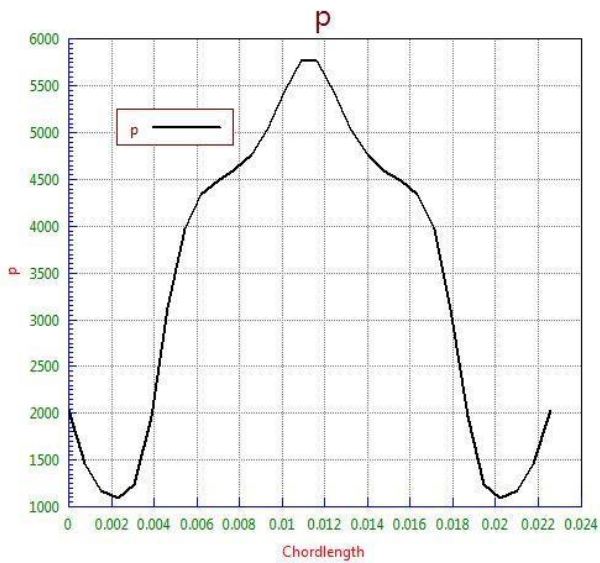


Figure 5-13. 30 Degree Nozzle Upper Wall Pressure Distribution

A third case was analyzed in which two 30 degree nozzles that are separated by a 50

distance of 3.3 cm instead of the proposed 2.3 cm. Figure 5-14 shows the velocity vector field for this scenario. The added 1.0 cm between the two nozzles is not sufficient to mitigate flow impingement of one nozzle on the other, as can be seen by the flow mixing at the midpoint between the two nozzles. However the pressure along the thruster structure wall is the lowest of all the simulated cases. The maximum pressure on the wall peaks at slightly above 4000 Pa as shown by Figure 5-16.

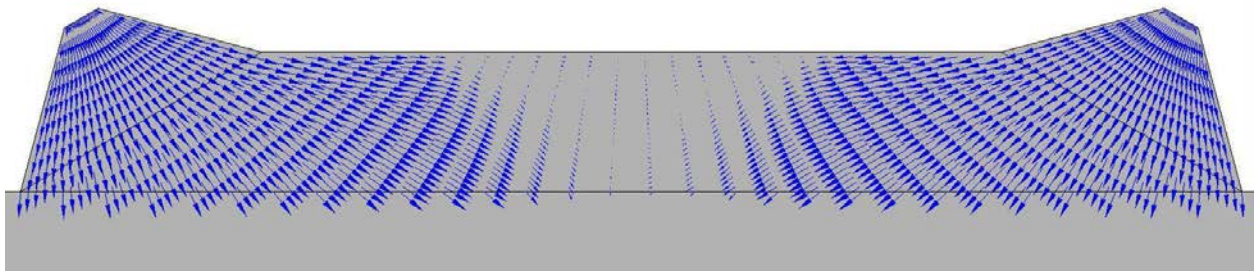


Figure 5-14. 30 Degree Extended Distance Velocity Vector Field

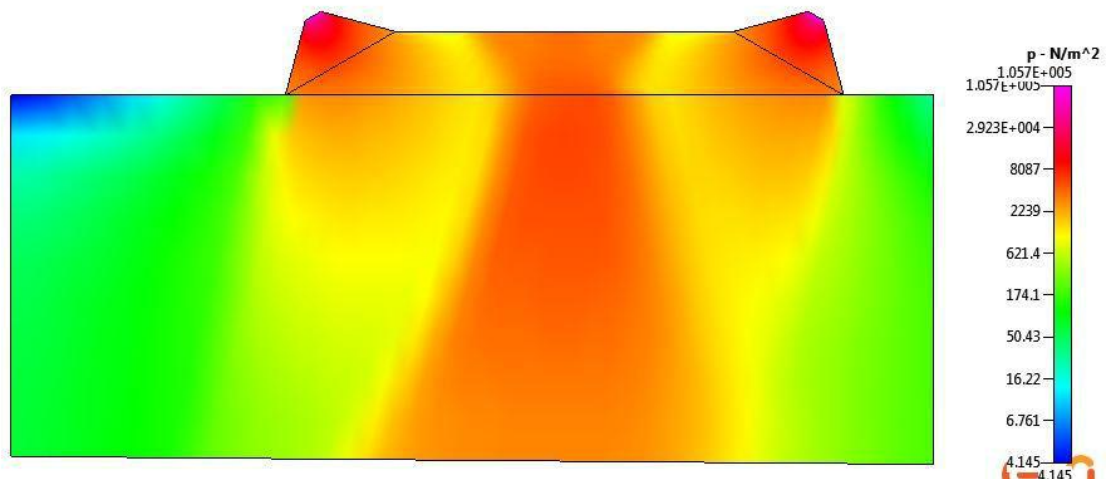


Figure 5-15. 30 Degree Extended Distance Pressure Distribution

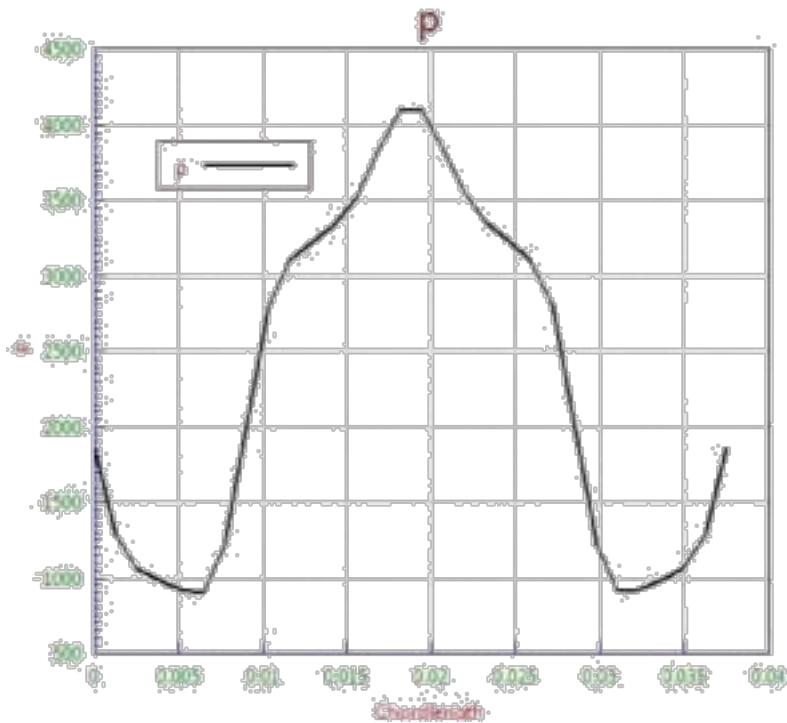


Figure 5-16. 30 Degree Nozzle Extended Distance Upper Wall Pressure Distribution

## 5.2 Alternative Nozzle Arrangement

The analysis provided by section 5.1 shows that any variation of the proposed arrangement from section 4.0 results in flow inefficiencies. These inefficiencies consist of pressure forces being exerted on the thruster structure as well as impingement between the two nozzle flows. One possible alternative for a four nozzle design is to place the nozzles at the corners of the thruster structure. This way all the propellant is directed away from the thruster system. A side-view of this is shown in Figure 5-17.

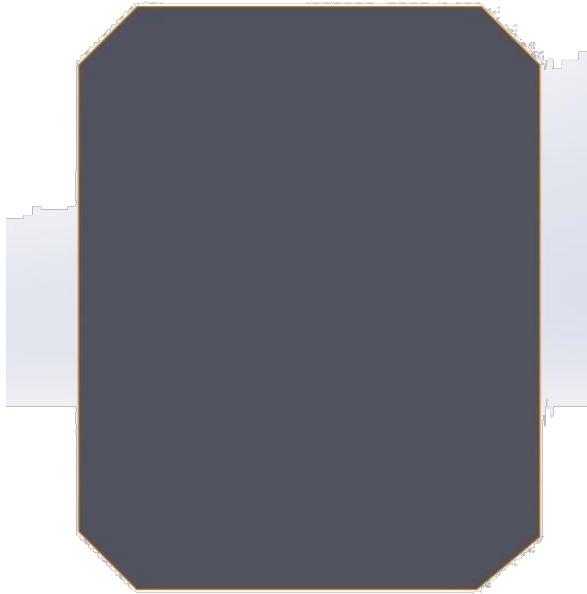


Figure 5-17. Alternative Nozzle Arrangement

## 6.0 CONCLUSION

Cubesats are currently one of the latest fields in spacecraft development. Their small size and cost allow many institutions to become involved with Cubesat projects. New improvements in additive manufacturing have the immense potential to further drive the simplicity and cost decrease of Cubesat system deployment. New Cubesat designs will require new propulsion systems. Propulsion capabilities are absolutely essential in increasing the mission proficiency of future Cubesats. This project has explored a possible future propulsion system arrangement. The system has four nozzles each capable of delivering 50 mN thrust at a theoretical vacuum specific impulse of  $60 \text{ s}^{-1}$  using DuPont 236fa refrigerant. The nozzles can be fired in any combination to initiate rotation

around three different axes. The thruster can hold 117 g of propellant and depending on the chosen material has a dry mass of around 80g. A system like this could be used to replace typical expensive and complex Cubesat propulsion systems, making it easier for institutions such as universities to rapidly produce and experiment with different designs.

## **6.1 Future Work**

The most important constraint on this design was the sizing of the valves. Valves in the future for vacuum applications could become smaller, allowing more flexible design sizing methodologies. Furthermore, new and improved additive materials could be explored as well as their compatibility with refrigerants and other similar inert propellants.

## 7.0 REFERENCES

1. Mueller, J., Hofer, R., & Ziemer, J., Survey of Propulsion Technologies Applicable to CubeSats, California Institute of Technology, Jet Propulsion Laboratory, May 3, 2010.
2. Small Satellite Propulsion Presentation, AstroRecon 2015, Arizona State University. 2015.
3. Parker, K. (2016). State-of-the-Art for Small Satellite Propulsion Systems. *4th Biennial Aerospace Systems Conference*.
4. UPrint SE Plus. (n.d.). Retrieved September 18, 2017, from <http://www.stratasys.com/3d-printers/uprint-se-plus>
5. Hinkey, D. (2008). A Novel Cold Gas Propulsion System for Nanosatellites and Picosatellites. *22nd Annual AIAA/USU Conference on Small Satellites*.
6. Arestie, S., Lightsey, G., & Hudson, B. (2012). Development of A Modular, Cold Gas Propulsion System for Small Satellite Applications. *Journal of Small Satellites*, 1(2), 63-74.
7. Nguyen, H., Kohler, J., & Stenmark, L. (2002). The Merits of Cold Gas Micropropulsion in State-of-the-Art Space Missions. *AIAA*.
8. Zandbergen, B. (2013). Micropropulsion Systems for Cubesats. *Von Karman Institute for Fluid Dynamics*.
9. Imken, T. K. (2014). *Design and Characterization of a Printed Spacecraft Cold Gas Thruster for Attitude Control*. University of Texas at Austin.

10. Moore, G., Holemans, W., Huang, A., Lee, J., McMullen, M., White, J., . . .  
Petterson, P. (2010). 3D Printing and MEMS Propulsion for the RAMPART  
2U Cubesat. *24th Annual AIAA/USU Conference on Small Satellites*.
11. Jerman, T. (2011.). *Calculating Cold Gas Microthruster Velocity Flow Using  
Finite Volume Analysis*. Lecture presented at Seminar in University of Ljubljana.
12. Larson, W., & Wertz, J. (Eds.). (1999). *Space Mission Analysis and Design*.  
El Segundo, CA: Microcosm.
13. [https://www.chemours.com/Refrigerants/en\\_US/assets/downloads/h77974\\_hfc23  
6fa\\_push.pdf](https://www.chemours.com/Refrigerants/en_US/assets/downloads/h77974_hfc236fa_push.pdf)
14. *NSTS 1700.7B (ISS ADDENDUM), Safety Policy and Requirements For  
Payloads Using the International Space Station (Rep.)*. (2003). NASA.
15. Refrigerant (R-134a) Properties, Uses, Storage, and Handling. (n.d.). Retrieved  
from [https://www.chemours.com/Refrigerants/en\\_US/assets/downloads/freon-  
134a-properties-uses-storage-handling.pdf](https://www.chemours.com/Refrigerants/en_US/assets/downloads/freon-134a-properties-uses-storage-handling.pdf)
16. Refrigerant (R-123) Properties, Uses, Storage, and Handling. (n.d.). Retrieved  
from [https://www.chemours.com/Refrigerants/en\\_US/assets/downloads/freon-  
123-properties-uses-storage-handling.pdf](https://www.chemours.com/Refrigerants/en_US/assets/downloads/freon-123-properties-uses-storage-handling.pdf)
17. DuPont HCFC-124 Properties, Uses, Storage, and Handling. (n.d.). Retrieved from  
[https://www.chemours.com/Refrigerants/en\\_US/assets/downloads/h62445\\_hcfc1  
24\\_push.pdf](https://www.chemours.com/Refrigerants/en_US/assets/downloads/h62445_hcfc124_push.pdf)

18. ABSplus Production-grade FDM 3D Printing Thermoplastic Material.  
(n.d.). Retrieved from <http://www.javelin-tech.com/3d-printer/materials/fdm-thermoplastic/absplus/>
19. Accura Bluestone (SLA) | 3D Systems. (n.d.). Retrieved from <https://www.3dsystems.com/materials/accura-bluestone>
20. Accura CeraMAX (SLA) | 3D Systems. (n.d.). Retrieved from <https://www.3dsystems.com/materials/accura-ceramax-composite>
21. Rasouli, F., & Williams, T. (2005). Application of Dispersion Modeling to Indoor Gas Release Scenarios. *Journal of the Air & Waste Management Association*, Mar.
22. Stevenson, T., & Lightsey, G. (n.d.). Design and Characterization of a 3D-Printed Attitude Control Thruster for an Interplanetary 6U CubeSat. *30th Annual AIAA Conference on Small Satellites*.